Epilepsy Research (2008) **79**, 173—186

journal homepage: www.elsevier.com/locate/epilepsyres

Emergent network topology at seizure onset in humans

Mark A. Kramer [a,*], **Eric D. Kolaczyk** [b], **Heidi E. Kirsch** [c]

[a] *Center for BioDynamics, 111 Cummington Street, Boston University, Boston, MA 02215, USA*
[b] *Department of Mathematics and Statistics, Boston University, Boston, MA 02215, USA*
[c] *Department of Neurology, University of California, San Francisco, CA 94143-0138, USA*

Received 11 August 2007; received in revised form 22 January 2008; accepted 7 February 2008
Available online 24 March 2008

KEYWORDS
Seizures;
Electrocorticogram;
Oscillations;
Correlation structure;
Network analysis;
Multivariate time series analysis

Summary Epilepsy — the world's most common serious brain disorder — is defined by recurrent unprovoked seizures that result from complex interactions between distributed neural populations. We explore some macroscopic characteristics of emergent ictal networks by considering intracranial recordings from human subjects with intractable epilepsy. For each seizure, we compute a simple measure of linear coupling between all electrode pairs (more than 2400) to define networks of interdependent electrodes during preictal and ictal time intervals. We analyze these networks by applying traditional measures from network analysis and identify statistically significant global and local changes in network topology. We find at seizure onset a diffuse breakdown in global coupling, and local changes indicative of increased throughput of specific cortical and subcortical regions. We conclude that network analysis yields measures to summarize the complicated coupling topology emergent at seizure onset. Using these measures, we can identify spatially localized brain regions that may facilitate seizures and may be potential targets for focal therapies.

Introduction

An important, perhaps fundamental, characteristic of seizures is the emergence of macroscopic order as observed in electrical activity recorded at the scalp and cortical surface. This order appears as, for example, ripples (Grenier et al., 2003) and beta frequency oscillations (Schiller et al., 1998) at seizure initiation, continues with increased synchronization during the middle phase of seizures (Schiff et al., 2005), and concludes as an abrupt cessation of activity (Schindler et al., 2007) at seizure termination. For focal epilepsies these macroscopic changes begin in spatially localized regions (i.e., the epileptogenic zone) and spread outward to affect other parts of the brain (Braizer, 1973). When focal epilepsy does not respond to seizure medications, the epileptogenic zone may be identified and surgically removed (Engel, 1996). Improved imaging and analysis techniques have refined but not substantially altered this procedure since the middle of the 20th century; a better understanding of how macroscopic order emerges

* Corresponding author. Tel.: +1 617 353 1493.
E-mail addresses: mak@bu.edu (M.A. Kramer), kolaczyk@math.bu.edu (E.D. Kolaczyk), Heidi.Kirsch@ucsf.edu (H.E. Kirsch).

0920-1211/$ — see front matter © 2008 Elsevier B.V. All rights reserved.
doi:10.1016/j.eplepsyres.2008.02.002

from the epileptogenic zone would help to refine surgical techniques and perhaps produce alternative therapies.

To characterize the spatiotemporal dynamics of ictal activity researchers have applied linear and nonlinear measures to recordings from individual electrodes (e.g., the power spectrum and correlation dimension) and from electrode pairs (e.g., coherence and phase synchronization). For a small number of electrodes, the latter results are easily displayed and interpreted. For example, one may compute the cross-correlation or coherence to infer properties of seizure propagation between a few electrode pairs (Braizer, 1973; Bertashius, 1991; Kramer et al., 2007). But, as the number of electrodes increases, interpreting the coupling results becomes much more complicated: the zero lag cross-correlation between all electrode pairs from an 8-by-8 subdural electrode grid produces $(64 \times 63)/2 = 2016$ values. How does one analyze the topological organization of these results and deduce the brain regions important for seizure facilitation or propagation? Similar challenges now face many neuroscientists as improved imaging and acquisition techniques yield ever-expanding quantities of multivariate, coupled data.

Network analysis provides many techniques to interpret such complicated coupling topologies. It has been used to characterize, for example, the network of electric power grids in the western United States (Watts and Strogatz, 1998) and the network of hyperlinks between different Internet web pages (Broder et al., 2000). In both cases, the network of interactions — among hundreds or millions of entities — is quite complex, yet has a topology whose structure is amenable to natural forms of summary and characterization. Recent studies suggest that networks derived from brain activity possess a ''small-world'' topology in which most connections are local and few are distant (Bassett and Bullmore, 2006; Ponten et al., 2007). Bispectral analysis of human intracranial EEG recordings has shown that the small-world characteristics of macroscopic neural activity increase at seizure onset (Wu et al., 2006), and simulation studies suggest that small-world networks better support phase synchronization and seizure-like activity (Percha et al., 2005; Netoff et al., 2004). Yet the role of small-world topology in seizures remains unclear; an *in vitro* model of stroke-induced epilepsy suggests that seizure-like discharges occur more frequency in random (not small-world) networks (Srinivas et al., 2007). In this manuscript, we attempt to further characterize the topological properties of the seizing human cortex. To do so, we apply a variety of network analysis measures to high-dimensional, multivariate electrocorticographic (ECoG) data recorded simultaneously from more than 70 electrodes in each of four human subjects with epilepsy. We show how — in this small group of subjects — the emergent coupling between electrodes changes at seizure onset and warrants further study. We also propose potential targets for therapeutic intervention identifiable only in the context of the entire network of coupled activity.

Methods

In this section we describe the human subject data and define the coupling measure and six measures of network analysis. For the primary subject, we show an example of the coupling between electrodes preceding and immediately following seizure onset, and note the qualitative differences. We apply the network analysis measures to quantify the changes in coupling that occur at seizure onset in the primary subject and in the aggregate group of four subjects in Results.

Recording equipment

Intracranial EEG were collected using the Viasys Nicolet BMSI 6000 NT Long Term Monitoring System (Viasys, Madison, WI, USA). Data were recorded from up to 128 channels at a fixed sampling rate of 400 Hz and bandpass filtered at a frequency range of 0.5—50 Hz (Butterworth filter) for later processing. A board-certified neurophysiologist (HEK) reviewed each dataset and verified the integrity of the recording. No artifacts (e.g., due to faulty electrode or recording cable performance) were identified.

Human subject data

Data were collected from four subjects with intractable epilepsy who had undergone electrode implantation as part of clinical care at the University of California, San Francisco (UCSF) Epilepsy Center. The implanted electrodes consisted of: a single 8-by-8 subdural electrode grid supplemented by subdural electrode strips and/or depth electrodes. All strip and grid electrodes were 4 mm diameter platinum—iridium discs embedded in 1.5 mm thick silastic sheet with 2.3 mm diameter exposed surfaces and 10 mm spacing between the discs. Depth electrodes were 1 mm in diameter and had four or six platinum contacts spaced 10 mm apart. To observe multiple seizures, physicians recorded ECoG data continuously for several days. For each subject, ictal data were extracted from the clinical record and analyzed for research purposes in accordance with UCSF and Boston University human subjects guidelines.

We begin with a description of the primary human subject (a 39-year-old right handed woman with medically refractory complex partial seizures) whose ECoG data we analyze in detail. Scalp video-EEG telemetry captured nine seizures that all arose from the left frontotemporal region (this was her dominant hemisphere for language) with some semiological features atypical for mesial temporal onset. Because of the relatively diffuse scalp localization and the origin in the language dominant hemisphere, it was decided to implant subdural electrodes to better determine focal ictal onset and to map functional brain regions. We show the craniotomy for this subject in Fig. 1a. In this figure, the left hemisphere of the brain is exposed. Approximately 44 of the 64 grid electrodes over the left frontotemporal region are visible; the remaining 20 electrodes are hidden below the edge of the craniotomy. The tails for the electrode strip (over the left suborbital frontal lobe) and of two, six-contact, left hippocampal depth electrodes are visible at the middle left and lower right portions of the figure, respectively; we indicate the location of these electrodes in the X-ray image shown in Fig. 1b. In Fig. 1c we show a three-dimensional reconstruction of the subject's cortex with the 8-by-8 electrode grid superimposed. For simplicity the strip and depth electrodes are not shown in this figure.

Physicians recorded ECoG data continuously from the primary subject for 5 days and detected nine seizures. Each seizure began near the distal end of both depth electrodes in the hippocampus and, approximately 15 s later, was observed on the (cortical) electrode grid. ECoG epochs containing eight of the patient's seizures and recorded simultaneously at 76 electrodes were extracted from the clinical record and saved for further analysis. (We note that one archived seizure data file was corrupted and no longer available for extraction, and that we omitted from analysis one set of six-contact depth electrodes that was saturated throughout the recording.)

For the primary subject, we analyze the eight recorded seizures in detail. We also apply three summary measures to three additional human subjects described below. The first was a 31-year-old

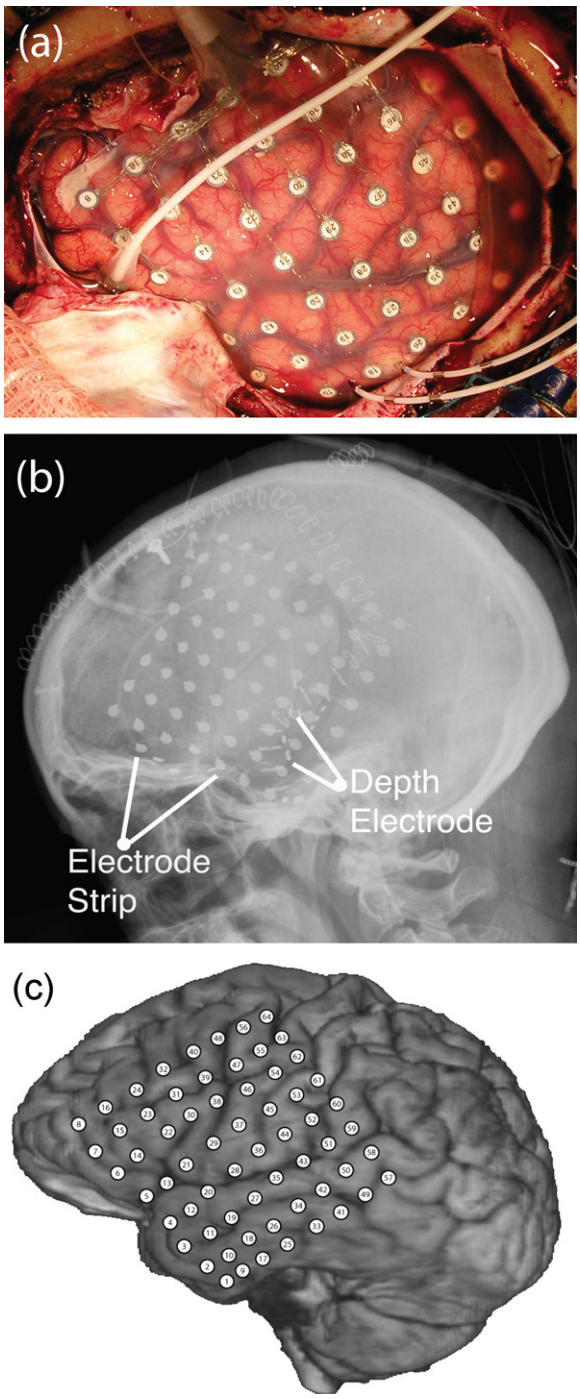

Figure 1 (a) Craniotomy for the primary subject. The frontal lobe is to the left in this figure and the left hemisphere is exposed. Visible are a portion of the 8-by-8 electrode grid, the insertion point of one subdural electrode strip (to the left) and two depth electrodes (at the bottom) that pierce the cortex orthogonal to its surface and record voltage activity from mesial temporal structures. (b) A skull X-ray of the subject following electrode implantation. We indicate the location of the (curved) electrode strip and the anterior depth electrode. (c) A three-dimensional reconstruction of the brain for this subject with the electrode grid superimposed.

right-handed woman with a 10-year history of medically refractory seizures. She had complex partial seizures with an aura of déjà vu and aphasia; they rarely secondarily generalized. Brain MRI was normal and routine EEG showed bitemporal sharp waves. She had scalp video-EEG telemetry and four seizures with posterior temporal origin were recorded. Physicians recorded ECoG data from an 8-by-8 electrode grid over her left frontotemporal region, and two, six-contact subdural electrode strips curled under her left anterior and left posterior temporal lobe for 14 days. Three seizures were initially captured. Midway through this recording period, the surgeon inserted an additional six-contact depth electrode into the left hippocampus. After this, three more seizures were recorded. Each seizure began in the distal end of the posterior left subtemporal electrode strip, and then spread to the distal end of the anterior subtemporal strip (as well as to the hippocampal depth electrode for the last three seizures). After a 60 s delay, seizure activity appeared on the electrode grid at the frontal portions of the superior and middle temporal gyri. We analyze three of the subject's seizures (two from the initial recording period and one from the later recording period). The patient went on to have a tailored resection of the left inferior temporal and fusiform gyri. She was initially seizure-free for 1.5 years but her seizures recurred after she tapered off one of her antiseizure medications.

The second additional subject was a 45-year-old right handed woman with medically intractable seizures since the age of 12, characterized by right body clonic movements out of sleep. Scalp video-EEG telemetry captured four seizures with broad left temporal onset but also showed frequent anterior frontal spikes. Brain MRI showed left perisylvian atrophy and cortical abnormalities in the same region, with a sclerotic left hippocampus. Given the breadth of the imaging abnormalities and the broad dominant hemisphere localization on scalp EEG, she went on to have implantation of an 8-by-8 electrode grid over her left frontotemporal region for seizure onset localization and for functional mapping. She also had a four-contact depth in her left amygdala, and a four-contact depth in her left hippocampus. Recording over 6 days captured three seizures. The first and third seizure were her typical seizure and arose from a small region of the left frontal lobe and then spread over several minutes to involve left temporal and parietal areas. The second seizure was clinically atypical for the patient and had a diffuse onset; we omit this seizure from analysis here. She had a resection of the left frontal lobe including orbitofrontal cortex to the frontal pole, sparing the gyrus rectus. The left mesial temporal structures were also removed. Pathological examination of the resected cortex was consistent with cortical dysplasia. Postoperatively she had some transient anomia that passed. She was seizure free for a brief period and then her seizures recurred, albeit at a reduced frequency from before.

The third additional subject was a 37-year-old ambidextrous man with refractory seizures since the age of seven. These are nocturnal events that involve right face and arm twitching. Scalp video-EEG telemetry was poorly lateralizing and localizing though semiology suggested left frontal origin. He went on to have implantation of an 8-by-8 electrode grid centered over his left parietal region, a four-contact left orbitofrontal strip, and a four-contact left subtemporal strip. Six typical seizures were recorded over 6 days, and all had onset in the suprasylvian frontal—parietal junction with low amplitude high-frequency activity followed several seconds later by a decrement lasting several tenths of a second, followed by high-amplitude, lower frequency activity in the same distribution. Three such seizures were analyzed for this study. The patient had a resection of a portion of the frontal operculum but was limited because the areas with epileptiform activity overlapped functional motor and speech regions. His course was complicated by a small venous infarct superior to the region of resection that caused some left hemiparesis and expressive aphasia that improved significantly over the ensuing months. He has been seizure free to date (1 year postoperatively).

Coupling measure

To apply techniques from network analysis we must first define the nodes and edges of an appropriate network. For the ECoG data of interest in this work the nodes are the individual electrodes. We define an edge to exist between two nodes if the voltage data recorded at the two nodes (i.e., the voltage data recorded at the two electrodes) are sufficiently coupled. There exist many measures to determine the coupling between two time series of voltage data (Pereda et al., 2005). Here we choose to use a simple measure of linear coupling: the cross-correlation. We chose this measure (and not more sophisticated synchronization techniques) because recent research suggests that — for the analysis of ictal and interictal (i.e., between seizure) ECoG data — linear measures perform similar to nonlinear measures (Mormann et al., 2005; Ansari-Asl et al., 2006).

We determine the coupling between two nodes by computing the cross-correlation between electrode pairs. To calculate the cross-correlation between two electrodes, we first bandpass filter the ECoG data at each electrode between 1 and 50 Hz. We then choose a 10 s interval and divide this interval into 20, 1 s segments, so that each segment overlaps the previous by 0.5 s. For example, if the 10 s interval extends from $t = 0$ to $t = 10$ s, then the duration of the first segment would be $t = \{0.0, 1.0\,\mathrm{s}\}$, the duration of the second segment would be $t = \{0.5, 1.5\,\mathrm{s}\}$, the third $t = \{1.0, 2.0\,\mathrm{s}\}$, and so on. Next, we compute the cross-correlation between the two electrodes within each 1 s segment. We choose to calculate the cross-correlation within the 1 s segments — rather than over the entire 10 s interval — to preserve (at least approximately) the stationarity of the ECoG data. We then examine the cross-correlation values for time shifts less than 250 ms and determine the maximum of the absolute value of the cross-correlation for each segment. We select the largest of these 20 values to define the coupling between the electrode pair. If the maximum of the absolute value of the cross-correlation exceeds 0.75 and occurs at a time shift less than 150 ms, then we declare the electrode pair coupled and connect the two electrodes (i.e., nodes) with an edge. (We have repeated the analysis using threshold values of 0.70 and 0.80 and found similar results for the network summary measures as we describe in Discussion). Otherwise we consider the electrode pair uncoupled and do not draw an edge between them. We note that an edge between two nodes could represent either a strong correlation or a strong anti-correlation between the voltage data recorded at the electrode pair, and that our network is defined to be unweighted (i.e., two nodes are either connected or not, with edge weights of 1 or 0, respectively).

We show a representation of the ECoG data as nodes and edges in Fig. 2a and b. To create Fig. 2a we compute the coupling measure as described above for a 10 s interval *preceding* the second seizure recorded from the primary subject; we call this the *preictal interval*. We indicate each node (i.e., electrode) with a filled circle in Fig. 2a; the orientation of the 8-by-8 electrode grid matches that shown in Fig. 1. We represent the six-contact electrode strip as the column of circles at the left of the subfigure and the six-contact depth electrode as the row of circles at the bottom of the figure. We connect each pair of coupled nodes with an edge drawn as a black curve. The topology of the network connections is quite complicated and not intuitively obvious.

We create Fig. 2b in a similar way, except that we choose the 10 s interval of ECoG data to begin immediately after onset of the second seizure; we call this the *ictal interval*. To define ictal onset in a reproducible way we implement the following procedure for each seizure from each subject. First, a board-certified neurologist and neurophysiologist (HEK) reviewed the ECoG recordings from each subject and identified the initial manifestation of rhythmic high frequency, low voltage focal activity thought to characterize the earliest appearance of a seizure (Fisher et al., 1992; Alarcon et al., 1995). A section of data including this high frequency, low amplitude, focal activity; the clinical seizure onset; and the clinical seizure cessation were extracted from the entire ECoG trace. Next, we divide the ECoG data recorded at each electrode into overlapping windows of 1 s duration as described above. Then we compute the average spectral power between 5 Hz and 15 Hz within each window. We chose this frequency band to encompasses the large amplitude, low frequency activity typically observed during intracranially recorded seizures (e.g., the after discharge period identified in (Wendling et al., 2003; Kramer et al., 2007). Finally, we average the resulting low frequency power spectra over all electrodes. We show the results of this procedure for the primary subject's second seizure in the upper trace of Fig. 2c and note the dramatic increase in low frequency power between 30 and 35 s compared to the initial portion of the trace. To define ictal onset, we identify by visual inspection this dramatic increase in the average low-frequency power; for each seizure studied, this increase corresponds to more than a 10-fold increase from the preictal interval. We indicate the ictal interval between the solid vertical lines in Fig. 2c. For reference, we also show ECoG data recorded at a single grid electrode (lower trace) and indicate the preictal interval between the dashed vertical lines. We note that other quantitative methods exist to define seizure onset (e.g., Schindler et al., 2007). An inspection of Fig. 2a and b suggests that the structure of the network changes at seizure onset; in particular, there are fewer edges drawn in Fig. 2b than in Fig. 2a.

We follow the same procedure to compute similar networks for each seizure from each subject. For the primary subject, the 10 s preictal intervals for the eight total seizures begin between 27 and 61 s (mean 39 s) before seizure onset. For all subjects, the 10 s preictal intervals for the sixteen total seizures begin between 22 and 180 s (mean 55 s) before seizure onset. We find (but do not show here) that each graph exhibits a complicated correlation structure like those shown in Fig. 2a and b. To quantify in a natural way the topology of the correlation structure, we employ six measures from network analysis: average path length, betweenness centralization, degree, closeness, clustering coefficient, and betweenness centrality. Two of these measures — the average path length and clustering coefficient — characterize the small-world properties of the seizing network, as recently described in (Ponten et al., 2007). The other measures (betweenness centrality in particular) characterize how information may propagate in the network. We provide brief definitions for these measures in the next subsection; more detailed discussions may be found in the literature (e.g., Wasserman and Faust, 1994; Nooy et al., 2005; Boccaletti et al., 2006).

Network analysis measures

Measures to characterize network topology are useful in many applications, for example, studies of information flow through the World Wide Web and monetary flow between nations. Here we employ six measures to characterize the network topology defined by the ECoG data. Two measures — the betweenness centralization and average path length — summarize the topological properties of the entire network. The other four measures — degree, closeness, clustering coefficient, and betweenness centrality — reveal changes specific to each node. We chose to apply six different measures because each illuminates different topological properties of the network. We compute each of these measures using the software package Pajek (Nooy et al., 2005) or algorithms written in the IDL software package (ITT Visual Information Solutions, Boulder, CO, USA) and study in detail how the topology of the graphs change at seizure onset in Results.

We begin with an illustrative example of network analysis. Consider the network defined by the airports and flight paths of a particular airline. In this example, the airports act as *nodes* in the network. An *edge* exists between two nodes (e.g., between Boston and San Francisco) if the airline flies between the two cities. Most flights involve stops at multiple nodes (i.e., no airline flies to all

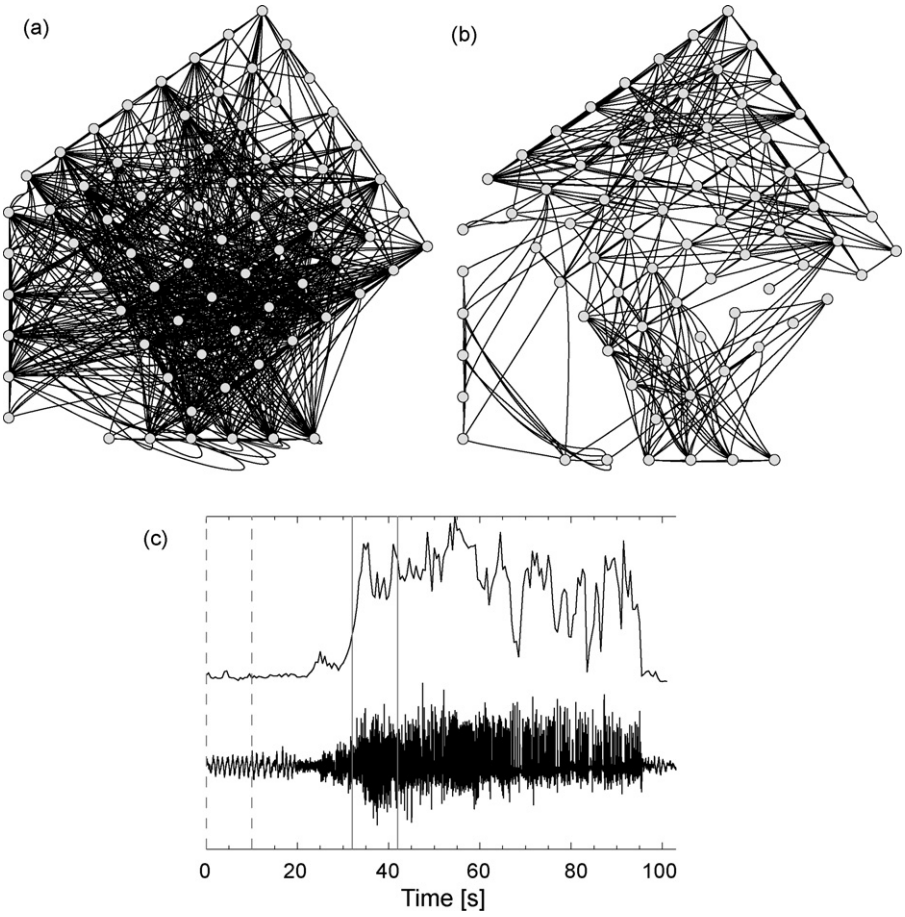

Figure 2 Two networks constructed from ECoG data recorded during the second seizure of the primary subject. We indicate the nodes (i.e., electrodes) as solid circles and draw edges between pairs of coupled nodes. We have positioned the 8-by-8 electrode grid to match the orientation in Fig. 1. The column of nodes at the left of each subfigure represents the six-contact orbitofrontal electrode strip, and the row of electrodes at the bottom of each figure represents the anterior six-contact depth electrode. (a) Network computed for the preictal interval. (b) Network computed for the ictal interval. We note that the number of edges appears to decrease during the ictal interval compared to the preictal interval. (c) ECoG data recorded at a single grid electrode (lower trace) and the average low-frequency power of all electrodes (upper trace). We indicate the 10 s preictal and ictal intervals between the vertical dashed lines and between the vertical solid lines, respectively. The vertical axis is arbitrary.

airports from each airport) so that the path between two nodes is often indirect. For example, the path from San Francisco to Oslo, Norway involves stops at both Boston and London. For this airline (and many others) the node London has particular importance. This node possesses a high *degree* (many edges end in London), *closeness* (most destinations are efficiently reached when travel begins in London), and *betweenness centrality*. To illustrate the latter measure, we note that the shortest path from San Francisco to Oslo involves a stop at London. In this case, the node London lies between the two nodes San Francisco and Oslo. In fact, the node London lies between many nodes, especially nodes on opposite sides of the Atlantic Ocean. Thus the betweenness centrality of the node London is high. If something were to happen to this node, the airline network would be severely disrupted. In general, if the betweenness centrality of a node is large, then this node represents a point of particular importance for communication in the network. Disrupt this node, and large regions of the network may no longer communicate. In what follows, we show that the betweenness centrality measure may be particularly important for assessing which brain regions propagate seizures.

We now define the network analysis measures. To illustrate these definitions and to introduce network analysis terminology we use the simple five node networks shown in Fig. 3. In Fig. 3a we have labeled two of the nodes j and k. To travel from node j to node k, we start at node j and traverse the graph by following a sequence of edges (the black lines) and nodes (the filled circles) until we reach node k. The length of this path is defined as the number of edges in the sequence, and the geodesic is the shortest path between nodes j and k. We define each edge to have length 1 so that, in this case, the geodesic has length 2. A measure to quantify the average length of geodesics throughout the entire network is the *average path length*. The average path length is defined as the mean length of geodesics over all pairs of reachable nodes in the network. (A pair of nodes is defined as reachable if a path exists between the two nodes.) In Fig. 3a—c the average path lengths are 1.6, 2.0, and 1.4, respectively. We note that this measure applies to the entire network, not to any node in particular.

The second measure we define is the *degree*. The degree of a node is the number of edges incident with the node. Because each edge connects two nodes, a node with high degree connects to many other nodes. In Fig. 3, we have labeled one node i in each network. The degree of this node is 4, 2, and 4 in the K-network, V-network, and B-network, respectively.

The third measure we consider is the *closeness*. The closeness of node i is defined as the number of nodes reachable from i divided by the summed distance to these reachable nodes. We note that,

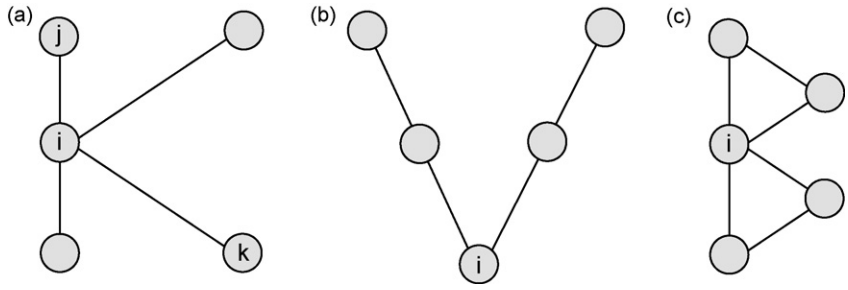

Figure 3 Simple five node networks: (a) the K-network, (b) the V-network and (c) the B-network.

in computing the closeness, only nodes reachable from *i* are considered. If the closeness of a node is large, then the distance from this node to other (reachable) nodes is small and information (e.g., money, gossip, voltage activity) may easily reach it. In Fig. 3 the node labeled *i* has the largest closeness value in each example. In the K-network and B-network, the node *i* is one edge from all other nodes, and in the V-network the node *i* is one edge from two nodes, and two edges from two nodes. The closeness of node *i* in the K-network and B-network is 1.0 and in the V-network is 0.67. In the former two networks, this node is directly linked (and therefore close) to all other nodes.

The *clustering coefficient* measures the number of triangles in which a node participates, relative to the total number in which it could participate, given its neighboring nodes. A triangle exists when three nodes (a triad) interconnect through edges. Applied to acquaintance networks, the clustering coefficient measures the likelihood of two individuals with a common friend also knowing one another (and thus completing the triangle). In both the K-network and V-network, the clustering coefficient of each node is zero; no triangles exist in these networks. In the B-network, the clustering coefficient of node *i* is 0.33 and 1.0 for all other nodes. The higher degree of node *i* decreases its clustering coefficient because this node could participate in many more triangles.

To define the last two measures — *betweenness centrality* and *betweenness centralization* — we consider a node *n* that exists in a graph. The betweenness centrality of *n* is a measure of the number of geodesics between all other nodes that pass through *n*. We note that betweenness centrality is a local measure that applies to each node in the network. Betweenness centralization is a summary measure of the variation in betweenness centrality over the entire network. Specifically, the betweenness centralization is the variation in the betweenness centrality of nodes divided by the maximum variation in the betweenness centrality values possible in a network of the same size (Nooy et al., 2005).

In the K-network node *i* has a betweenness centrality value of 1.0; all geodesics between other nodes in the network pass through node *i*. The exterior nodes — which do not serve as intermediate nodes along any geodesics in the network — have zero betweenness centrality. The entire K-network has a betweenness centralization value of 1.0; this network possesses the maximum possible variation in betweenness centrality for a network of five nodes. In the V-network three nodes possess a nonzero betweenness centrality (with values of 0.5, 0.5, and 0.67). The betweenness centralization for the entire network has a value of 0.42, less than that of the K-network because variation in the betweenness centrality of the nodes in the V-network is reduced. Finally, for the B-network, the betweenness centralization is 1.0 and betweenness centrality of node *i* is 1.0. No other nodes in the B-network are intermediate to any geodesic; therefore, these nodes possess a betweenness centrality of zero. In general, if the betweenness centrality of an individual node is large, then this node represents a point of particular importance for ''communication'' — or similar notions of information exchange — in the network. For example, if we remove node *i* from the K-network, we disrupt all communication in that network. In what follows, we show that the betweenness centrality measure may be particularly important for assessing which brain regions propagate seizures.

Results

In this section we apply the six network analysis measures to the ECoG data recorded from the primary human subject. We show that the two summary measures — the average path length and the betweenness centralization — increase at seizure onset, and that the degree and closeness of most electrodes tend to decrease at seizure onset. The betweenness centrality and clustering coefficient results do not exhibit such uniform change. We summarize these results in Table 1. We then apply three global measures to the ECoG data recorded from the 8-by-8 electrode grids of four human subjects. We again find that all three global measures increase at seizure onset.

Analysis of ECoG data: primary human subject

We begin by considering the two global measures: the average path length and betweenness centralization. An inspection of the complicated network topology shown in Fig. 2 suggests that the average path length increases at

Table 1 Summary of the network analysis results for the primary human subject

Measure	Change at seizure onset
Average path length	↑
Betweenness centralization	↑
Betweenness centrality	↑↓
Clustering coefficient	↑↓
Closeness	↓
Degree	↓

We list the measures in the first column and the change at seizure onset observed for each measure (averaged over eight seizures) in the second column. The average path length and betweenness centralization are summary measures of network topology; the betweenness centrality, clustering coefficient, closeness, and degree are local measures that apply to each node. The degree and closeness decrease for nearly all electrodes. Both increases and decreases occur for the betweenness centrality and clustering coefficient, depending on the node.

seizure onset; fewer edges exist in the ictal network, and we expect that the shortest path between any two nodes is less direct and therefore longer compared to the corresponding path in the preictal network. We compute the average path length for the preictal and ictal intervals determined for the eight seizures and find values of 2.0 ± 0.4 and 2.6 ± 0.2, respectively. The difference in the means of these values is statistically significant ($p < 0.005$). We compute the betweenness centralization of the preictal and ictal networks, average the results from the eight seizures, and find values of 0.05 ± 0.05 and 0.14 ± 0.04, respectively. The difference in the means of these values is also statistically significant ($p < 0.005$). We conclude that both the average path length and betweenness centralization increase at seizure onset. The latter result indicates that the betweenness centrality of the nodes becomes less uniform at seizure onset; some nodes acquire larger betweenness centrality values while others acquire smaller values. We note that — although the number of edges decreases at seizure onset — nearly all nodes remain connected to the network. At most four nodes separate from the network completely, and for seven preictal and six ictal intervals one or fewer nodes separate. The remaining nodes form a single connected component in which each node is reachable from every other node. We also note that — for each individual seizure — the average path length increases, and for seven (of eight) seizures the betweenness centralization increases at ictal onset. Both measures provide a single scalar value that summarizes the complicated preictal and ictal network topologies.

An inspection of Fig. 2 also suggests that the degree of most nodes decreases at seizure onset; we observe fewer edges in the ictal network compared to the preictal network. To quantify this change, we compute the degree of each node during the preictal and ictal intervals. We show the results for the preictal and ictal intervals in Fig. 4a and b, respectively. In each subfigure (and those that follow) we arrange the nodes as in Fig. 2 and indicate the value of the measure by the radius of the circle. To determine the change in degree at seizure onset, we compute the difference in degree at each node between the ictal and preictal states by subtracting the preictal values from the ictal values. We average these differences over the eight seizures and show the results in Fig. 4c. In this figure, the radius of the circle indicates the magnitude of the degree difference, and the shading the sign. If the average degree of a node *decreases* at seizure onset, then the node is white; otherwise, we shade the node grey. We use this shading scheme in all figures that follow. We find that — for all nodes — the average degree decreases or remains nearly unchanged at seizure onset. The magnitude of this decrease tends to be larger for nodes in the lower half of the figure. We interpret the wide-spread decrease in degree to indicate that the connectivity of the network tends to decrease at seizure onset, especially for nodes in the lower half of the figure. The degree measure allows us to interpret the complicated network topology (illustrated in Fig. 2) as reflected locally in each node in a natural and obvious way.

For the fourth measure we compute the closeness of each node during the preictal and ictal intervals and show the results in Fig. 5a and b, respectively. We position the nodes as in the previous figures, and we indicate the value of the closeness — averaged over the eight seizures — by the radius of the circle. We average the difference in closeness between the ictal and preictal states over the eight seizures and plot the results in Fig. 5c. We find that, for nearly all nodes, the average closeness decreases at seizure onset. The magnitude of this decrease tends to be larger for nodes in the lower half of the figure. Like the diffuse decrease observed in degree, the wide-spread decrease in closeness may result from disconnection — and therefore increased distance — between most nodes at seizure onset.

The fifth measure we compute is the clustering coefficient. We show the results for the preictal and ictal intervals

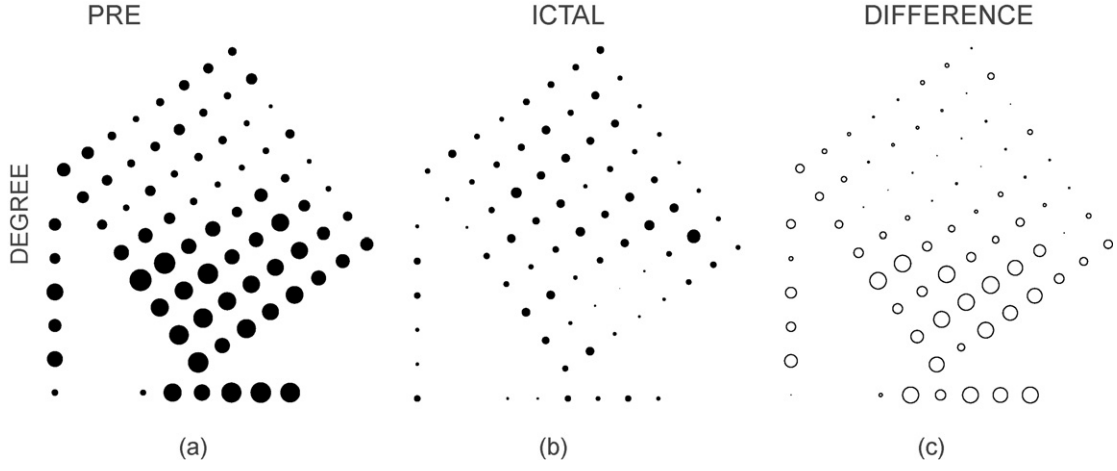

Figure 4 Results for the degree calculation of the primary subject. We arrange the nodes in the same way as in Fig. 2. We indicate the value of the degree by the radius of the circle during (a) the preictal and (b) the ictal intervals. We show how the degree changes at seizure onset in (c). In this subfigure, the radius of the circle indicates the magnitude of the degree difference and the shading the sign; a white (grey) circle denotes a decrease (increase) in degree at seizure onset. The largest radius indicates a degree of 40 in all three subfigures. We find that the average degree of most nodes decreases at seizure onset.

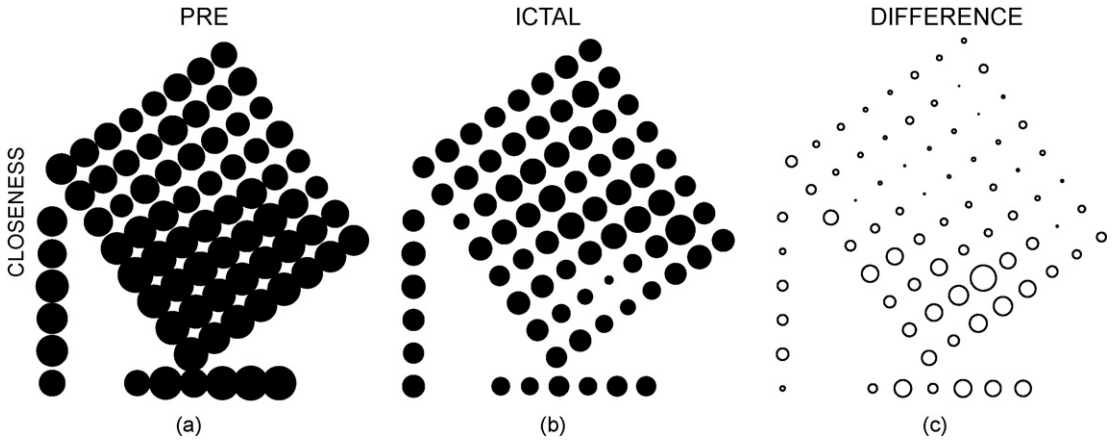

Figure 5 Results for the closeness calculation of the primary subject. We arrange and shade the nodes in the same way as for the previous figures. We indicate the value of the closeness by the radius of the circle during (a) the preictal and (b) the ictal intervals. We show how the closeness changes at seizure onset in (c). The largest radius indicates a closeness of 0.65 in all three subfigures. We find that the average closeness of most nodes decreases at seizure onset.

in Fig. 6a and b, respectively, and for the difference in Fig. 6c. We find that the clustering coefficient of most nodes decreases at seizure onset, but differs from the pattern of decrease observed in degree and closeness in two ways. First, we observe a dispersed spatial pattern of decreased clustering coefficients. The largest decreases in clustering coefficient are scattered over the nodes, not clumped in one region of the grid. Second, not all nodes decrease in clustering coefficient at seizure onset. Of the 76 nodes, 32 become more clustered at seizure onset. To determine which nodes display a statistically significant change in clustering coefficient in a manner that controls for the rate of false discoveries, we compute the q value of the results (Storey and Tibshirani, 2003). At the level of $q = 0.05$, we find zero nodes with a significant decrease in clustering coefficient. If we instead set $q = 0.20$, we find a significant decrease at three nodes (of which we expect $3 \times 0.2 < 1$ to be a falsely declared decrease). We mark these nodes in Fig. 6c. We conclude that the disconnection at seizure onset destroys some — but not many — complete triangles in the network in an inhomogeneous way.

The final measure we consider is the betweenness centrality. We show the average results for the preictal and ictal intervals in Fig. 7a and b. We plot the average difference results in Fig. 7c and find that the betweenness centrality of some nodes increases at seizure onset, while other nodes exhibit no change or a decrease in betweenness centrality. We note that the direction of change in betweenness centrality, like the clustering coefficient, is not uniform across nodes. At a level of $q = 0.05$, we find 13 nodes with a significant change in betweenness centrality (of which we therefore expect $13 \times 0.05 = 0.65 < 1$ out of these 13 to be a falsely declared increase). We mark these nodes with single or double asterisks.

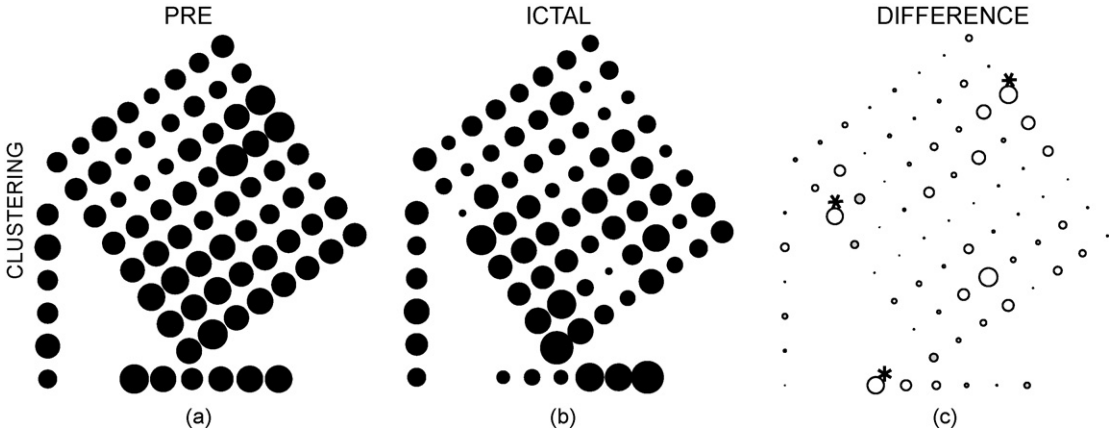

Figure 6 Results for the clustering coefficient of the primary subject. We indicate the value of the clustering coefficient by the radius of the circle during (a) the preictal and (b) the ictal intervals. We show how the clustering coefficient changes at seizure onset in (c). The largest radius indicates a clustering coefficient of 0.80 in all three subfigures. We find a significant decrease at the $p = 0.20$ level at three nodes (each marked with an asterisk).

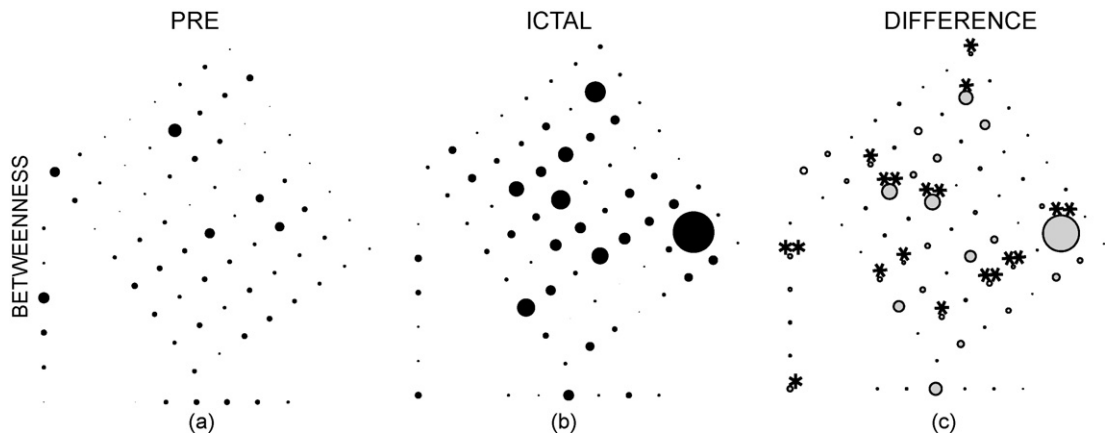

Figure 7 Results of the betweenness centrality analysis of the primary subject. We indicate the value of the betweenness centrality by the radius of the circle during (a) the preictal and (b) the ictal intervals. We show how the betweenness centrality changes at seizure onset in (c). We mark the 13 electrodes that exhibit a statistically significant increase in betweenness centrality with asterisks. The double asterisks indicate nodes that exhibit a statistically significant increase for coupling thresholds of 0.70, 0.75, and 0.80. The largest radius indicates a betweenness centrality of 0.13.

We summarize the network analysis results for the primary subject in Table 1.

Additional human subjects

In the previous section, we considered the network analysis of ECoG data collected from a single human subject. In this section, we analyze ECoG data recorded from the primary subject plus three additional human subjects. For each subject, we choose to analyze only the data recorded from the 8-by-8 electrode grid (located on the left frontotemporal area for two subjects and on the left frontotemporoparietal area for two subjects). We apply to these grid data the cross-correlation measure defined in Methods to determine the coupling between electrode pairs and establish two networks (preictal and ictal) for each seizure recorded from each subject. We then analyze the 16 total seizures recorded from the four subjects by applying three summary measures of network topology. We chose to apply only summary measures for two reasons. First, we do not expect the electrical activity of seizures to propagate in the same way for different subjects. We may find, for example, decreased degree at ictal onset in the lower half of the electrode grid for one subject (as in Fig. 4) and in the center of the grid for another subject. Therefore, although the electrode grids cover approximately the same cortical regions we cannot easily compare local measures (such as degree or betweenness centrality) between subjects. Second, the summary measures provide a single, scalar result for each seizure from each subject. These measures summarize the complicated network topology in a way that facilitates a formal statistical comparison across subjects of changes occurring during the transition to seizure.

We find, based on the measurements from the four human subjects, that increases in both the average path length and betweenness centralization are associated with seizure onset. In particular, increases of 0.6662 in average path length and 0.055 in betweenness centralization were found significant at the 0.005 level ($p < 0.005$), controlling for variation among subjects, based on a mixed effects ANOVA analysis. A robust version of the analysis (with observations replaced by their ranks) yielded similar results.

As a third summary measure, we compute the small-world-ness of the preictal and ictal intervals (Humphries et al., 2006). To do so, we first construct for each seizure and subject 50 corresponding random graphs with 64 nodes and the number of edges equivalent to that observed in the data. Then, for each seizure and interval, we compute the average path length and average clustering coefficient (averaged over the 64 nodes) of the random graphs and divide the average path length (average clustering coefficient) of the data by the average path length (average clustering coefficient) of the corresponding random graphs. The small-world-ness is the ratio of the clustering coefficient ratio to the average path length ratio (Humphries et al., 2006). We find for the preictal and ictal intervals average small-world-ness values of 2.0 ± 0.8 and 3.2 ± 1.1, respectively. The increase in small-world-ness at ictal onset was found significant at the 0.001 level (i.e., $0.0005 < p < 0.001$), controlling for variation among subjects, based on a mixed effects ANOVA analysis. A robust version of the analysis (with observations replaced by their ranks) yielded similar results.

We have also examined the four local measures (degree, closeness, clustering coefficient, and betweenness centrality) applied to the three additional subjects and found results qualitatively similar to those listed in Table 1. Namely, we find that the degree and closeness — averaged over the seizures recorded from a subject — tend to decrease at seizure onset for nearly all electrodes. The clustering coefficient and betweenness centrality tend to increase for some electrodes and decrease for others. In Fig. 8 we show all four measures applied to all four subjects. For the additional subjects, we do not plot the electrode positions according to the anatomical locations. Instead we simply show the average results recorded from the electrode grid and strip or depth electrodes. Because we analyze only two or three seizures from each of these subjects, we cannot perform a meaningful statistical analysis of an individual subject's results.

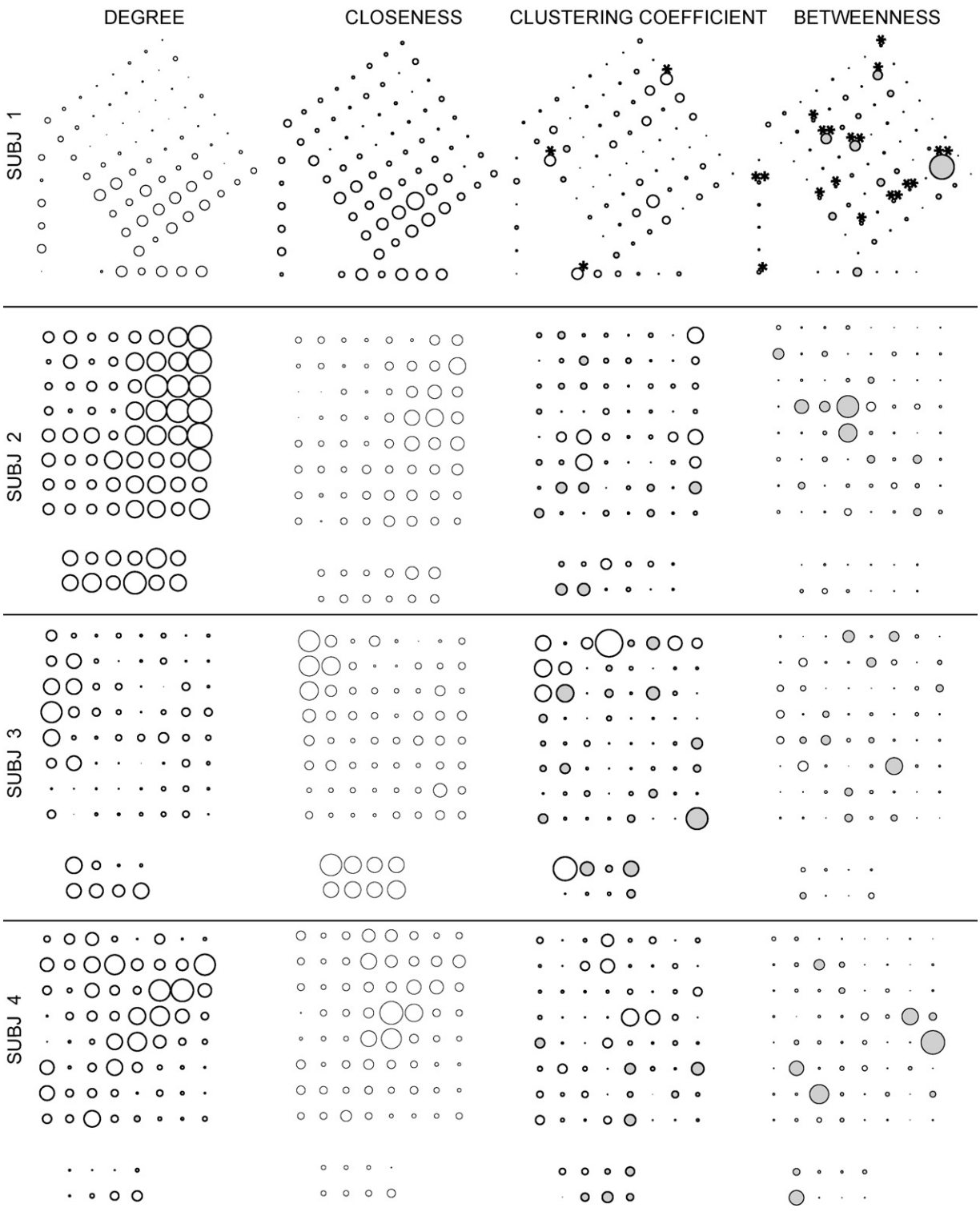

Figure 8 The change in the four local measures observed at ictal onset in the four human subjects. Each column corresponds to a measure, from left to right: degree, closeness, clustering coefficient, and betweenness centrality. Each row corresponds to a subject. We show the results for the primary subject in the top row, and the additional subjects in the other three rows. For the additional subjects, we show the results for the 8-by-8 electrode grid and the additional strip and depth electrodes. The electrode positions do not indicate anatomical locations. The shading scheme follows that used in the previous figures.

Discussion

We have applied six measures from network analysis — average path length, betweenness centralization, degree, closeness, clustering coefficient, and betweenness centrality — to high-dimensional, multivariate ECoG data recorded from a seizing human subject. We found that the two summary measures (average path length and betweenness centralization) increased at seizure onset. We also found that — for most electrodes — degree and closeness decreased at seizure onset. Changes in the clustering coefficient and the betweenness centrality tended to vary among electrodes at seizure onset; in particular some electrodes exhibited a sharp increase in betweenness centrality, while others increased or decreased only slightly. We summarized these results in Table 1. We applied the network analysis to three additional human subjects and showed that the average path length and betweenness centralization tended to increase at seizure onset. In addition, we found that the small-world-ness increased at ictal onset, in agreement with some previous studies (e.g., Netoff et al., 2004; Wu et al., 2006), but not others (Srinivas et al., 2007).

We note the decrease in coupling observed at seizure onset. This decoupling appeared qualitatively as a thinning of edges in the network graphs and quantitatively as a decrease in degree and closeness of nearly all nodes. The magnitude of this decrease in both measures was not spatially uniform. For the primary subject, the largest decreases occurred at electrodes in the lower half of the 8-by-8 electrode grid and for the strip and depth electrodes. The effect of the decreased coupling may be to reveal those brain regions facilitating the seizure. In fact, for the primary subject, most nodes with significant increases in betweenness centrality displayed only small decreases in degree and closeness (compare Figs. 4c and 5c with Fig. 7c). In addition, some of these same nodes displayed deceases in clustering coefficient. We interpret the latter results to suggest that at ictal onset some nodes stay connected to the network while the neighbors of these nodes disconnect (and thus destroy previously present triangles). Similar decreases in coupling (i.e., decorrelation or desynchronization) during seizure were recently observed in rat hippocampal slices (Netoff and Schiff, 2002) and in man (Wendling et al., 2003).

In Results, we presented the mean changes in network measures averaged over the eight seizures of the primary subject. For each seizure we have also examined the preictal and ictal values of the average path length and found a consistent result, namely an increase in average path length at ictal onset. For the betweenness centralization, we find an increase at seizure onset in seven of eight seizures. We interpret these results to suggest a consistent change in network topology for each seizure. We have also visually inspected the changes in degree and betweenness centrality for each seizure of the primary subject. We find a qualitatively similar pattern for each seizure. Specifically, nodes near the center and right of the grid appear to increase in betweenness centrality and nodes near the lower portion of the grid appear to decrease in degree at seizure onset, as we show in Fig. 9.

In constructing the network representations of the data, we created an edge between two nodes if the ECoG data recorded at the two electrodes were sufficiently coupled. We defined ''sufficient coupling'' as the maximum of the absolute value of the cross-correlation exceeding 0.75. The value of this coupling threshold is important. If we make the threshold too large (e.g., 0.995), then we find almost no edges in the network. A comparison between the preictal and ictal states — each with zero edges — is therefore meaningless. If we make the threshold too small (e.g., 0.005), then we find edges between every node in the network and again render meaningless any comparison between the preictal and ictal states. Therefore, we chose a coupling threshold between these two extreme values. We have repeated the analysis with threshold values of 0.70 and 0.80 and found significant increases in the average path length ($p < 0.01$) and near significant increases in the betweenness centralization ($p < 0.06$) at seizure onset. Moreover, of the 13 electrodes that exhibit a significant increase ($q = 0.05$ level) in betweenness centrality at seizure onset, six are identical for thresholds of 0.70, 0.75, and 0.80. We mark these six nodes with a double asterisk in Fig. 7c. An improved method to chose the coupling threshold would be of use—ideally, one that would maximize the quality of information in the network graph representation relative to its intended usage.

By choosing a fixed correlation threshold, we created preictal and ictal networks with different numbers of edges (compare Fig. 2a and b). We created the networks in this way because decreased coupling — and therefore a thinning of edges — appears to be a physiological characteristic of the transition from preictal to ictal activity (Netoff and Schiff, 2002; Wendling et al., 2003). If instead we create preictal and ictal networks with the same number of edges (by adapting the threshold in each case) we ignore this characteristic but establish networks with more comparable topology. We have repeated our analysis of the primary subject choosing the 500 largest cross-correlation values to establish the same number of edges during each interval and for each seizure. For the degree, closeness, clustering coefficient, and betweenness centrality, we find results qualitatively similar to those for the fixed coupling threshold of 0.75 (data not shown). Yet, for the average path length and betweenness centralization we find no significant difference between the preictal and ictal states.

In computing the coupling results we made four important assumptions. First, we used the cross-correlation between electrode pairs to establish the coupling measure. We chose to use this measure because, for the analysis of ECoG data during seizure, linear measures seem to perform just as well as nonlinear measures (Ansari-Asl et al., 2006; Mormann et al., 2005). Use of a different measure (e.g., phase synchronization) or filtering of the data into different frequency bands may change the characteristics of the network, but the same network analysis would still be applicable. Second, we identified the approximate time of ictal onset to coincide with clinical and visible ECoG changes as determined by a clinical neurophysiologist (HEK) and refined this approximation by computing the average low frequency power of all electrodes in the ECoG data. We note that seizures often begin with a brief interval of focal low amplitude, high frequency activity; in this work, we chose to focus instead on the large amplitude, rhythmic activity that arises as seizures are fully underway. Future studies that consider the topology of additional time intervals (e.g., interictal, post-ictal) would be of use. Third, in our analysis we have not

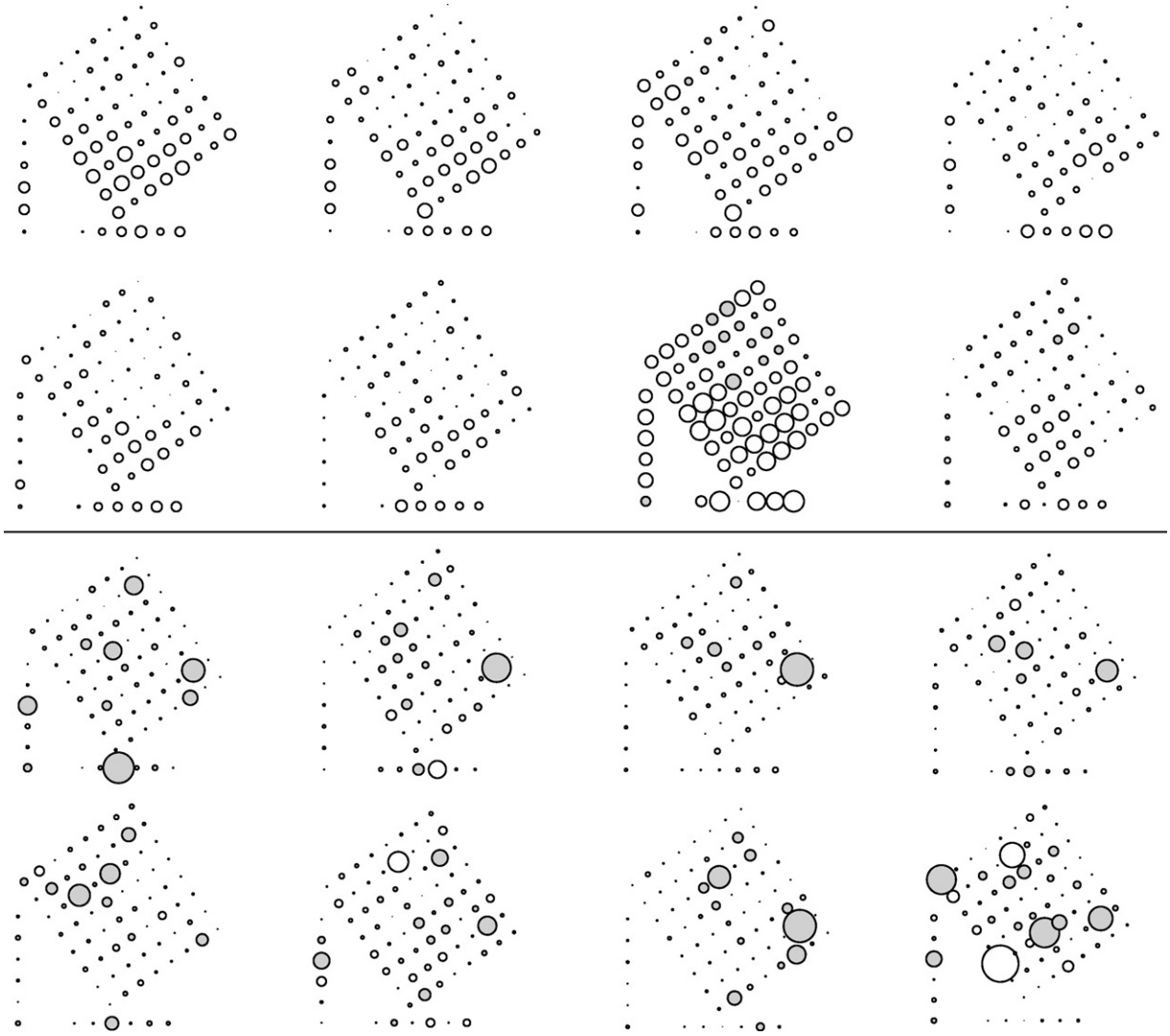

Figure 9 The change in degree (upper half of figure) and betweenness centrality (lower half of figure) at ictal onset computed for each seizure of the primary subject. Visual inspection suggests qualitatively similar changes occur for each seizure. In particular, we note that nodes in the lower half of the electrode grid tend to decrease in degree, and that nodes near the center and right of the grid tend to increase in betweenness centrality at each seizure onset.

considered the temporal relationship between electrodes. Perhaps by considering the time shift at which the strongest coupling occurs we could infer how the voltage activity propagates over the entire cortex during seizure and study the dynamic network topology (Kramer et al., 2007). Fourth, we assume that coupling between electrodes indicates communication between brain areas. This may not be the case if, for example, a common source drives similar activity in two disconnected neural populations. In future analyses, application of imaging or neurophysiological techniques to test for anatomical or functional connectivity would be of use.

We conclude by suggesting that network analysis measures may indicate targets for therapeutic intervention. We identified at seizure onset two changes in network topology: (1) decreased connectivity of many nodes, and (2) increased betweenness centrality of few nodes. For the former, the disconnection is apparent in the average degree and closeness measures for the primary subject shown in Figs. 4c and 5c. We propose that a possible anti-seizure treatment would functionally ''reconnect'' the disconnected regions. This might occur through regional application of drugs that enhance synaptic transmission (e.g., 4-aminopyridine). We note an important alternative interpretation: the higher correlation during the preictal period may instigate the decorrelating seizure. In this case, reconnecting cortical regions may shorten but not prevent the seizure. For (2), we identify 13 nodes with statistically significant increases in betweenness centrality in Fig. 7c. We suggest that these nodes may facilitate seizure activity and that their disruption (by focal responsive electrical stimulation (Gluckman et al., 2001), drug delivery (Stein et al., 2000) or cooling (Rothman et al., 2005)) could prevent or abort ictal activity. These nodes might also serve as candidates for resective surgery especially when the epileptogenic focus cannot be removed (for example, when the seizure initi-

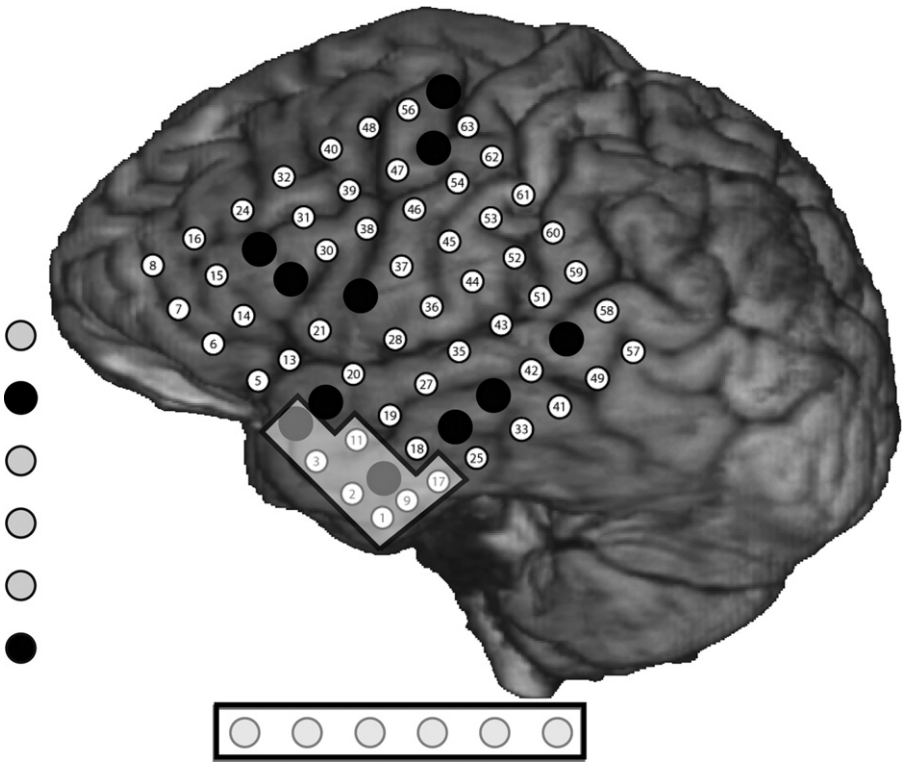

Figure 10 Comparison of therapeutic targets and resected tissue of the primary subject. We indicate the nodes identified as therapeutic targets with filled black circles, and the nodes resected during an anterior temporal lobectomy within the shaded white boxes. Only two nodes that displayed a statistically significant increase in betweenness centrality were removed.

ates in eloquent cortex or when the seizure is nonfocal and widespread, as is often the case in neocortical seizures).

To suggest the utility of the prospective therapeutic targets, we show in Fig. 10 the three-dimensional reconstruction of the primary subject's cortex and indicate both the prospective therapeutic targets and the cortical region removed during the subject's anterior temporal lobectomy. We find that — of the 13 nodes identified to increase in betweenness centrality at seizure onset — only 2 nodes were resected. The resection instead targeted nodes exhibiting large decreases in degree and closeness at seizure onset. Two months following surgery, the primary subject continued to experience recurrent seizures, although less frequently than pre-operatively. Perhaps the reduction in seizure frequency resulted from removing nodes with dense connectivity (and therefore higher degree) during the preictal interval. Would the resection of additional nodes (or electrical stimulation of nodes contacting eloquent cortex) improve the surgical outcome? A longitudinal study in humans comparing surgical outcome with network analysis measures, or invasive recordings in a simple physiological model of epilepsy, would help disprove or validate the technique.

We note that both therapies — diffuse drug application to enhance connectivity or localized electrical stimulation or resection to reduce connectivity — emerge from analysis of the entire network. We could not identify these potential targets by studying each electrode individually or in pairs; instead, we must analyze each node within the context of the coupled network. In both cases we target emergent properties of the network for therapy (Faingold, 2004). We are, of course, cautious in identifying new types of therapy; these ideas must be tested using longitudinal studies that, for example, correlate brain removal of regions exhibiting increased betweenness centrality with postoperative seizure freedom. The identification of prospective nodes as therapeutic targets is limited by the number and extent of clinical recording electrodes; the 76 electrodes from the primary subject record from only a small portion of the cortex. Electrodes positioned at different locations might identify more robust targets. In addition, seizures may propagate along many different paths so that the disruption of one communication hub might facilitate others and, thus, not prevent ictal onset.

The network analysis techniques we present here are applicable to many other complex datasets used in neuroscience, such as MEG and microelectrode arrays. All that is required is the establishment of nodes (e.g., MEG sensors or microelectrodes) and edges determined from any type of coupling metric (Section 6.4 of Boccaletti et al., 2006). Network analysis provides measures to summarize complicated network topology in a natural way and reveals characteristics of the network not obtainable from the study of individual nodes alone, and thus is of increasing utility to neuroscience.

Acknowledgements

We are grateful to Nicholas M. Barbaro, M.D., for electrode placement and surgical management, to the fellow and attending staff of the UCSF Epilepsy Center for medical

management, and to Sarang S. Dalal for assistance with a figure. EDK was supported in part by ONR award N00014-06-1-0096.

References

Alarcon, G., Binnie, C.D., Elwes, R.D., Polkey, C.E., 1995. Power spectrum and intracranial EEG patterns at seizure onset in partial epilepsy. Electroencephalogr. Clin. Neurophysiol. 94, 326—337.

Ansari-Asl, K., Senhadji, L., Bellanger, J., Wendling, F., 2006. Quantitative evaluation of linear and nonlinear methods characterizing interdependencies between brain signals. Phys. Rev. E 74, 031916.

Bassett, D.S., Bullmore, E., 2006. Small-world brain networks. Neuroscientist 12, 512—523.

Bertashius, K.M., 1991. Propagation of human complex-partial seizures—a correlation-analysis. Electroencephalogr. Clin. Neurophysiol. 78, 333—340.

Boccaletti, S., Latora, V., Moreno, Y., Chavez, M., Hwang, D.U., 2006. Complex networks: structure and dynamics. Phys. Rep. 424, 175—308.

Braizer, M.A., 1973. Electrical seizure discharge within the humn brain: the problem of spread. In: Braizer, M.A. (Ed.), Epilepsy, Its Phenomena in Man. Academic Press, New York.

Broder, A., Kumar, R., Maghoul, F., Raghavan, P., Rajagopalan, S., Stata, R., Tomkins, A., Wiener, J., 2000. Graph structure in the web. Comput. Networks 33, 309—320.

Engel, J., 1996. Current concepts—surgery for seizures. N. Engl. J. Med. 334, 647—652.

Faingold, C.L., 2004. Emergent properties of CNS neuronal networks as targets for pharmacology: application to anticonvulsant drug action. Prog. Neurobiol. 72, 55—85.

Fisher, R.S., Webber, W.R., Lesser, R.P., Arroyo, S., Uematsu, S., 1992. High-frequency EEG activity at the start of seizures. J. Clin. Neurophysiol. 9, 441—448.

Gluckman, B.J., Nguyen, H., Weinstein, S.L., Schiff, S.J., 2001. Adaptive electric field control of epileptic seizures. J. Neurosci. 21, 590—600.

Grenier, F., Timofeev, I., Steriade, M., 2003. Neocortical very fast oscillations (ripples, 80—200 Hz) during seizures: intracellular correlates. J. Neurophysiol. 89, 841—852.

Humphries, M.D., Gurney, K., Prescott, T.J., 2006. The brainstem reticular formation is a small-world, not scale-free, network. Proc. R. Soc. B 273, 503—511.

Kramer, M.A., Szeri, A.J., Sleigh, J.W., Kirsch, H.E., 2007. Mechanisms of seizure propagation in a cortical model. J. Comp. Neurosci. 22, 63—80.

Mormann, F., Kreuz, T., Rieke, C., Andrzejak, R.G., Kraskov, A., David, P., Elger, C.E., Lehnertz, K., 2005. On the predictability of epileptic seizures. Clin. Neurophysiol. 116, 569—587.

Netoff, T.I., Clewley, R., Arno, S., Keck, T., White, J.A., 2004. Epilepsy in small-world networks. J. Neurosci. 24, 8075—8083.

Netoff, T.I., Schiff, S.J., 2002. Decreased neuronal synchronization during experimental seizures. J. Neurosci. 22, 7297—7307.

Nooy, W.D., Mrvar, A., Batagelj, V., 2005. Exploratory Social Network Analysis with Pajek. Cambridge University Press, New York.

Percha, B., Dzakpasu, R., Zochowski, M., Parent, J., 2005. Transition from local to global phase synchrony in small world neural network and its possible implications for epilepsy. Phys. Rev. E 72, 031909.

Pereda, E., Quiroga, R.Q., Bhattacharya, J., 2005. Nonlinear multivariate analysis of neurophysiological signals. Prog. Neurobiol. 77, 1—37.

Ponten, S.C., Bartolomei, F., Stam, C.J., 2007. Small-world networks and epilepsy: graph theoretical analysis of intracerebrally recorded mesial temporal lobe seizures. Clin. Neurophysiol. 118, 918—927.

Rothman, S.M., Smyth, M.D., Yang, X.F., Peterson, G.P., 2005. Focal cooling for epilepsy: an alternative therapy that might actually work. Epilepsy Behav. 7, 214—221.

Schiff, S.J., Sauer, T., Kumar, R., Weinstein, S.L., 2005. Neuronal spatiotemporal pattern discrimination: the dynamical evolution of seizures. Neuroimage 28, 1043—1055.

Schiller, Y., Cascino, G.D., Busacker, N.E., Sharbrough, F.W., 1998. Characterization and comparison of local onset and remote propagated electrographic seizures recorded with intracranial electrodes. Epilepsia 39, 380—388.

Schindler, K., Leung, H., Elger, C.E., Lehnertz, K., 2007. Assessing seizure dynamics by analyzing the correlation structure of multichannel intracranial EEG. Brain 130, 65—77.

Stein, A.G., Eder, H.G., Blum, D.E., Drachev, A., Fisher, R.S., 2000. An automated drug delivery system for focal epilepsy. Epilepsy Res. 39, 103—114.

Storey, J.D., Tibshirani, R., 2003. Statistical significance for genomewide studies. Proc. Natl. Acad. Sci. U.S.A. 100, 9440—9445.

Srinivas, K.V., Jain, R., Saurav, S., Sikdar, S.K., 2007. Small-word network topology of hippocampal neuronal network is lost, in an in vitro glutamate injury model of epilepsy. Eur. J. Neurosci. 25, 3276—3286.

Wasserman, S., Faust, K., 1994. Social Network Analysis: Methods and Applications. Cambridge University Press, New York.

Watts, D.J., Strogatz, S.H., 1998. Collective dynamics of small-world networks. Nature 393, 440—442.

Wendling, F., Bartolomei, F., Bellanger, J.J., Bourien, J., Chauvel, P., 2003. Epileptic fast intracerebral EEG activity: evidence for spatial decorrelation at seizure onset. Brain 126, 1449—1459.

Wu, H., Li, X., Guan, X., 2006. Networking property during epileptic seizure with multi-channel EEG recordings. In: Wang, J., et al. (Eds.), Lecture Notes in Computer Science, vol. 3976, pp. 573—578.